Acta Crystallographica Section D
Biological Crystallography
ISSN 0907-4449

Laboratory multiple-crystal X-ray topography and reciprocal-space mapping of protein crystals: influence of impurities on crystal perfection

Z. W. Hu,[a]* B. R. Thomas[a,b] and A. A. Chernov[a]

[a]Universities Space Research Association, NASA/Marshall Space Flight Center, Huntsville, AL 35812, USA, and [b]Center for Microgravity Materials Research, University of Alabama in Huntsville, Huntsville, AL 35899, USA

Correspondence e-mail: zhengwei.hu@msfc.nasa.gov

Received 12 January 2001
Accepted 3 April 2001

Double-axis multiple-crystal X-ray topography, rocking-curve measurements and triple-axis reciprocal-space mapping have been combined to characterize protein crystals using a laboratory source. Crystals of lysozyme and lysozyme crystals doped with acetylated lysozyme impurities were examined. It was shown that the incorporation of acetylated lysozyme into crystals of lysozyme induces mosaic domains that are responsible for the broadening and/or splitting of rocking curves and diffraction-space maps along the direction normal to the reciprocal-lattice vector, while the overall elastic lattice strain of the impurity-doped crystals does not appear to be appreciable in high angular resolution reciprocal-space maps. Multiple-crystal monochromatic X-ray topography, which is highly sensitive to lattice distortions, was used to reveal the spatial distribution of mosaic domains in crystals which correlates with the diffraction features in reciprocal space. Discussions of the influence of acetylated lysozyme on crystal perfection are given in terms of our observations.

1. Introduction

The subject of structural imperfections in biological macromolecular crystals remains intriguing because of the need to produce better quality crystals for structural analysis. The extent and types of growth-induced defects are largely governed by solution properties, crystallization conditions and growth processes (Rosenberger *et al.*, 1996; Durbin & Feher, 1996; Chayen *et al.*, 1996; Chernov, 1997, 1999; McPherson, 1998; McPherson *et al.*, 1999). The extent to which crystalline imperfections influence the diffraction resolution depends on the amount and the nature of the defects present. In general terms, crystal defects distinguish themselves from the rest of near-perfect lattice parts by producing diffuse scattering in the background and, in a more striking effect, by modifying the sharp Bragg peaks about the reciprocal-lattice nodes. This degrades the diffraction resolution and the structural quality.

In addition to diffraction-resolution and *B*-factor measurements, there are two types of X-ray methods normally used for the characterization of the structural quality of macromolecular crystals. The first method mainly deals with crystal mosaicity using double-axis rocking-curve measurements (Shaikevitch & Kam, 1981; Helliwell, 1988; Snell *et al.*, 1995; Fourme *et al.*, 1995; Ng *et al.*, 1997) and triple-axis diffraction profile analysis (Dobrianov *et al.*, 1998) or diffraction-space mapping (Fewster, 1997; Volz & Matyi, 2000; Boggon *et al.*, 2000). The second method refers to X-ray topography (Lang, 1976; Tanner, 1976; Klapper, 1991; Bowen & Tanner, 1998), by which defect structures, in particular the spatial distribution of mosaic domains *etc.*, can be mapped out in terms of the

variation of the diffracted intensity across the beam (Fourme *et al.*, 1995; Stojanoff & Siddons, 1996; Stojanoff *et al.*, 1997; Dobrianov *et al.*, 1998; Otalora *et al.*, 1999; Boggon *et al.*, 2000). Indeed, combined X-ray topography and diffraction measurements have been used to provide better assessment of the structural quality of protein crystals using synchrotron sources (*e.g.* Fourme *et al.*, 1995; Dobrianov *et al.*, 1998; Boggon *et al.*, 2000).

The creation of stress and mosaicity by the trapping of impurities has been generally analyzed by Chernov (1997, 1999). The effects of macromolecular impurities such as lysozyme dimer (Carter *et al.*, 1999; Judge *et al.*, 2000), ovotransferrin and turkey egg-white lysozyme (Caylor *et al.*, 1999) on the quality and diffraction resolution of hen egg-white lysozyme (HEWL) crystals have been experimentally investigated. Despite this progress, it remains unclear as a whole if and how each type of impurity affects the crystal quality. To date, most X-ray characterization work on macromolecular crystals has been carried out at synchrotron X-ray sources, which offer the intensity to probe the diffraction problem at a higher resolution, although reciprocal-space mapping of lysozyme crystals has recently been reported using laboratory X-ray sources (Fewster, 1997; Volz & Matyi, 1999, 2000; Snell *et al.*, 1999). In this paper, we present a combined laboratory X-ray topography, rocking-curve and reciprocal-space mapping study of crystals of HEWL and of HEWL crystals incorporating acetylated lysozyme molecules (as a microheterogeneous impurity). The results demonstrate the potential of home-laboratory X-ray diffraction techniques to become a useful and routine tool to assess the quality of macromolecular crystals as they are for quality control of semiconductor crystals and devices.

2. Experimental details

Diffraction and topographic experiments were performed on a rotating-anode-based high angular resolution X-ray diffraction system (Snell *et al.*, 1999). The diffractometer (Fig. 1) is equipped with a four-bounce two-crystal Ge(220) Bartel-type monochromator and a triple-bounce Ge(220) analyzer. This X-ray optical configuration produces not only a well collimated incident beam in the horizontal scattering plane, but also a tailless feature of the output beam conditioned by the monochromator and analyzer (Fewster, 1996). The narrow band pass defined by the Bartel-type four-bounce monochromator has a negligible broadening effect on the width of rocking curves measured for low scattering angle (*i.e.* low diffraction resolution) geometry. The tailless feature from the monochromator and analyzer is particularly useful in the study of diffuse scattering from samples in reciprocal space (Hu *et al.*, 1998). Rocking curves were measured using a double-axis configuration (without invoking the analyzer) and rocking ω (Fig. 1). In the triple-axis configuration (Fig. 1), reciprocal-space maps around lattice nodes were measured by driving the analyzer and detector (the 2θ arm) at twice the rate of the sample rotation ω in the $\omega/2\theta$ direction over a number of scans each offset by a step of $\delta\omega$ in the ω scan direction. As shown in Fig. 2, the $\omega/2\theta$ (or q_z) scan is a radial scan that is parallel to the reciprocal-lattice vector and the ω (or q_x) scan is a lateral scan over the reflection plane that is perpendicular to the reciprocal-lattice node within a small scan range. The angular dependence of the intensity along $\omega/2\theta$ is related to the relative variation of the lattice spacing of the reflection plane, whereas the distribution of the intensity along ω is sensitive to the component of lattice tilts (mosaicity) with respect to the goniometer axis, lateral correlation lengths and crystal curvature. These cannot be differentiated in double-

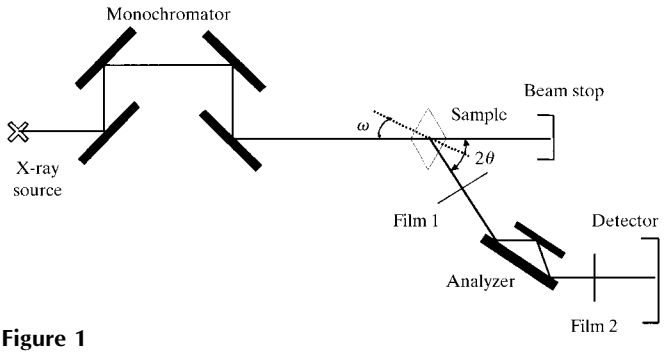

Figure 1
Schematic drawing of a multiple-crystal and multiple-reflection triple-axis X-ray diffractometer. Rocking curves are measured using the double-axis configuration (without the analyzer) and by rocking ω. Reciprocal-space maps are collected using the triple-axis system. Film 1 position is used for high spatial resolution X-ray topographs.

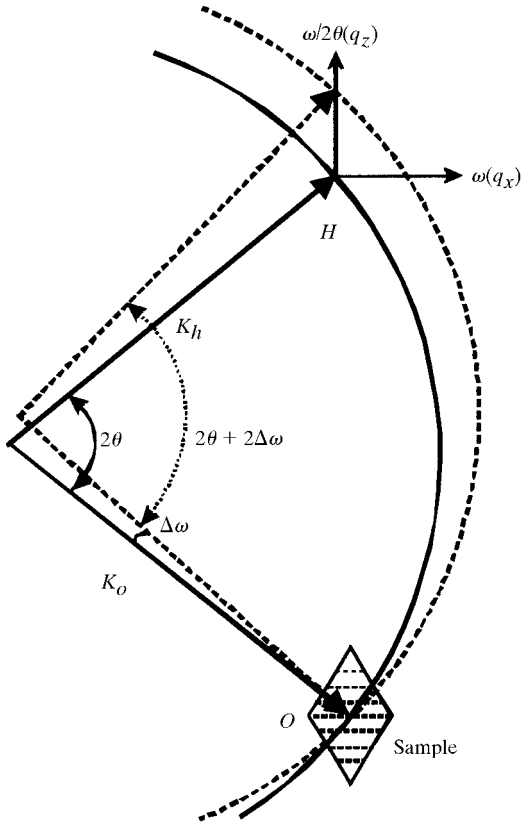

Figure 2
Ewald sphere illustration of the triple-axis ω and $\omega/2\theta$ scans for the transmission diffraction geometry.

axis rocking curves in which the intensity received is intrinsically integrated over a large Ewald sphere area (indeed, rocking-curve measurements can be preformed *via* rocking either ω or $\omega/2\theta$ in most cases). Reflections were measured using Cu $K\alpha 1$ radiation and at $2\theta_B \simeq 6.4^\circ$ (the angular position of the tetragonal lysozyme crystal 440). X-ray diffraction images were recorded on Ilford L4 nuclear emulsion plates taken in a high spatial resolution topographic imaging mode (Hu *et al.*, 1996). Samples, which were held in place inside X-ray quartz capillaries, were bathed in the incident X-ray beam for diffraction and imaging measurements.

The HEWL crystals utilized for this work were those obtained from the study by Thomas & Chernov (2001). Briefly, Seikagaku HEWL (Thomas *et al.*, 1996) was crystallized at three supersaturations: 20, 30 and 40 mg ml^{-1} in 50 m*M* sodium acetate buffer pH 4.5 with 4% sodium chloride. Crystals grown as experimental controls containing no acetylated HEWL (Thomas *et al.*, 1996, 1998) were compared with those which contained the most acetylated (lowest positive charge) HEWL impurity, termed 'impurity A'. Crystallization conditions were identical for both with compensation for a small additional amount of sodium chloride (50 m*M*) present in the impurity A sample added to the controls to maintain identical supersaturation. Impurity A was added to the HEWL crystallizing solution at a concentration of 0.76 mg ml^{-1}. Foreign protein impurities are not well incorporated into protein crystals (Carter *et al.*, 1999); however, impurity A is a deliberately created microheterogeneous impurity and is preferentially incorporated into HEWL crystals with a partitioning coefficient $K = 2.15 \pm 0.13$ (Thomas & Chernov, 2001). Because the amount of added impurity is small and the effects on a protein crystal may be subtle, every effort is made to create identical crystals in controls and in treated samples except for the one variable impurity A concentration.

3. Results and discussions

Fig. 3(*a*) presents an X-ray topograph of lysozyme crystal 1 taken on the peak position of the rocking curve (Fig. 3*b*). A well shaped crystal feature is preserved in the topograph, being indicative of no appreciable lattice distortions existing inside the crystal. Diffraction contrast is rather uniform across the sample and no single dislocation is discernable in the X-ray topograph. A diffraction-space map is shown in Fig. 3(*c*) in which a well defined sharp Bragg peak appears. One of the features of the map is that the intensity falls more slowly along the lateral (ω) scan direction than in the radial ($\omega/2\theta$) scan. The FWHM of the ω-scan diffraction profile is $\sim$0.0037° (Fig. 3*d*), which is directly related to the distribution of lattice tilts, *i.e.* the lattice mosaicity. The FWHM of the radial-scan

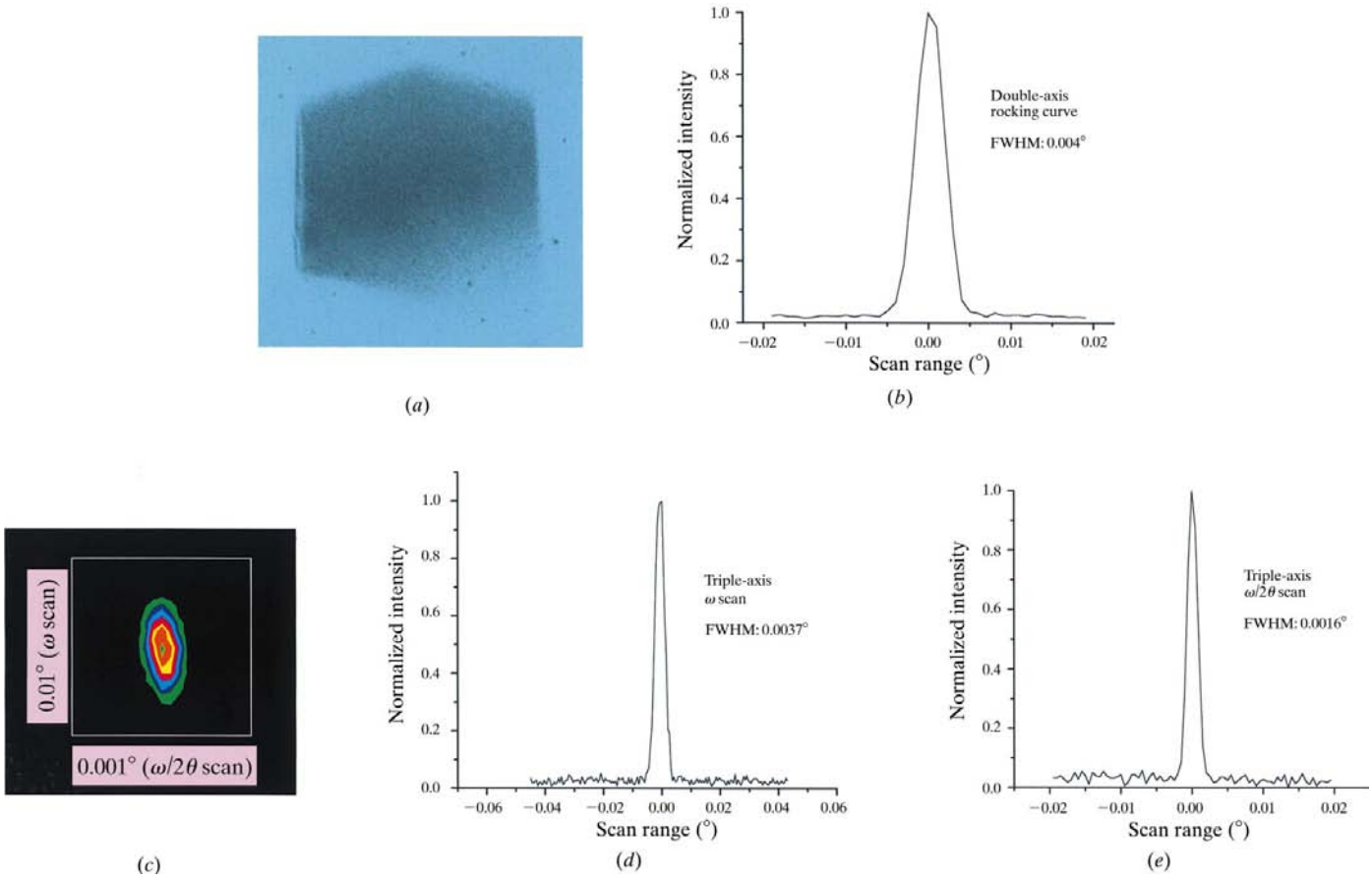

Figure 3
X-ray topographic and diffraction characterization of lysozyme crystal 1. (*a*) X-ray topograph, (*b*) double-axis rocking curve, (*c*) triple-axis reciprocal-space map, (*d*) triple-axis ω scan, (*e*) triple-axis $\omega/2\theta$ scan.

diffraction profile is extremely narrow, ∼0.0016°, which is essentially instrumentally limited (Hu *et al.*, 1998, 1999). An X-ray topograph of sample 2 that was grown from a solution containing acetylated lysozyme 2.5%(*w*/*w*) [∼5%(*w*/*w*) in the crystal; Thomas & Chernov, 2001)] is given in Fig. 4(*a*), in which mosaic blocks or domains are discernable although the crystal is optically perfect. The FWHM of the rocking curve (Fig. 4*b*) is ∼0.0054°. The corresponding diffraction-space map is shown in Fig. 4(*c*) in which the intensity is extended only along the ω-scan direction. Figs. 4(*d*) and 4(*e*) are projections of the diffraction-space map along the ω and $\omega/2\theta$ directions, respectively. The overall FWHM is ∼0.0054° for the ω scan, the same as that of the rocking curve in Fig. 4(*b*), while the diffraction profile is actually composed of subpeaks that are from the different mosaic domains observed in the topograph (Fig. 4*a*). The FWHM of the $\omega/2\theta$ scan is ∼0.0017°, almost the same as that of sample 1. That is, no appreciable lattice strain is observed within the instrumental resolution. Fig. 5(*a*) presents an X-ray diffraction image of sample 3 grown from a solution containing acetylated lysozyme 3.5%(*w*/*w*) (∼8% in the crystal; Thomas & Chernov, 2001). The intensity appears extremely non-uniform across the sample, as expected from the rocking curve (Fig. 5*b*). The reciprocal-space map given in Fig. 5(*c*) shows an extensive distribution of the scattering intensity along ω consisting of several subpeaks. This is consistent with what is revealed in the diffraction image (Fig. 5*a*), in which the crystal is found to be composed of small mosaic domains, each slightly rotated from one another. Only those domains that are oriented in the Bragg diffraction condition diffracted strongly and therefore appear black in Fig. 5(*a*). The overall FWHM of the ω scan (Fig. 5*d*) is extremely high, more than 90 arcsec, but the FWHM of the $\omega/2\theta$ scan (Fig. 5*e*) remains extremely narrow, ∼0.0017°.

The diffraction profiles (Figs. 3*b*, 3*c* and 3*d*) from the lysozyme crystal sample 1 are highly symmetric and sharp, following a Gaussian shape. An instrumental function from the monochromator is Gaussian with a FWHM $\simeq$ 0.0033°. By taking a correction for instrumental broadening, the mosaic width is ∼0.002°. The angular dependence of the intensity along ω for the impurity-doped lysozyme crystals cannot be described well by a pure Gaussian function. For example, Fig. 4(*d*) from sample 2 follows a pseudo-Voigt lineshape (Hu *et al.*, 1999), with a profile-shape (Lorentzian) factor of ∼0.53. The mosaic values of sample 2 and 3 are ∼0.004° and ∼0.025°, respectively. Note that the size of the domains affects the diffraction-profile shape, but does not appreciably influence the widths of the profiles in the present cases. A highly non-

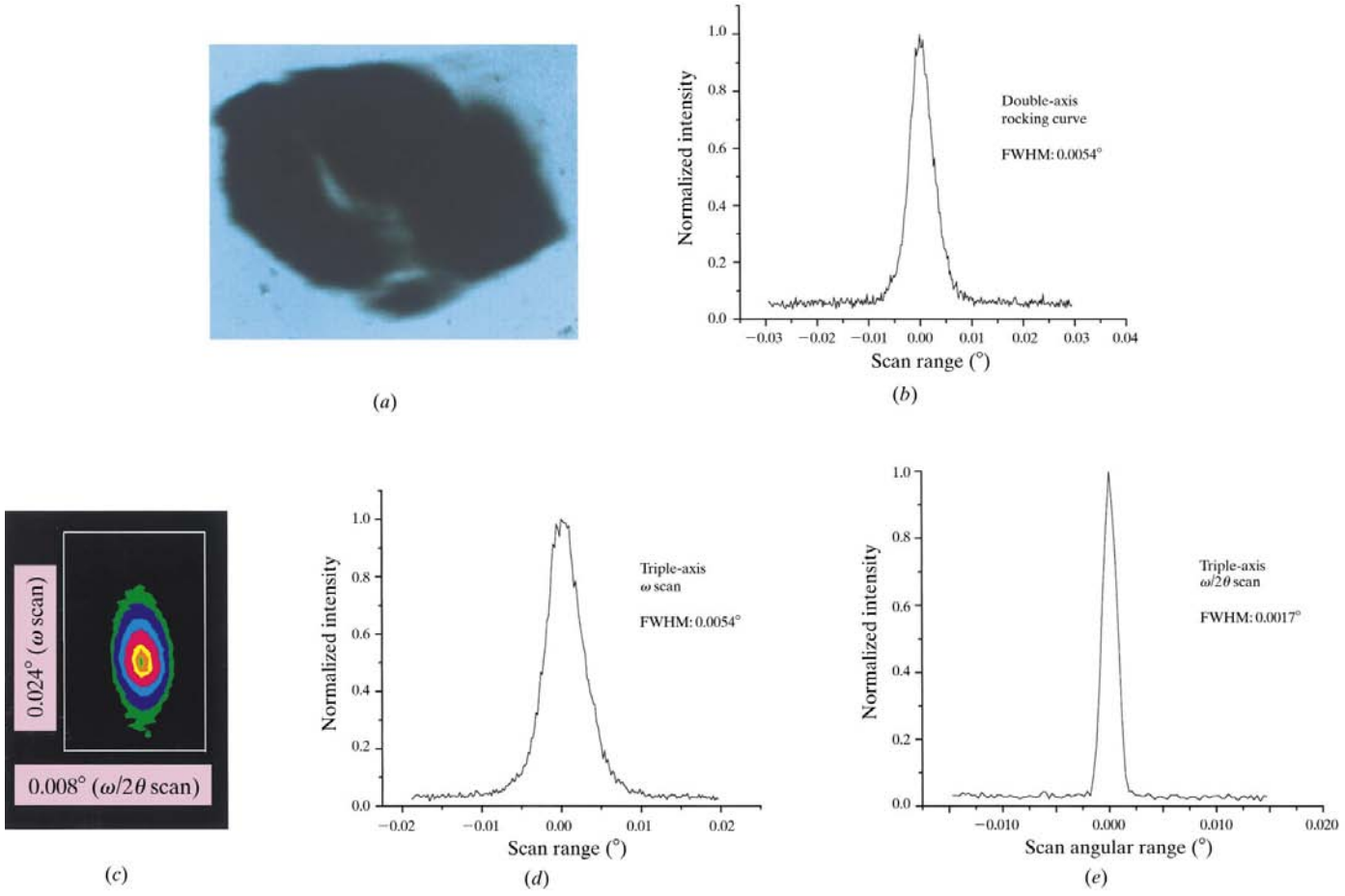

Figure 4
X-ray topographic and diffraction characterization of acetylated lysozyme doped lysozyme crystal 2. (*a*) X-ray topograph, (*b*) double-axis rocking curve, (*c*) triple-axis reciprocal-space map, (*d*) triple-axis ω scan, (*e*) triple-axis $\omega/2\theta$ scan.

Gaussian mosaic distribution was observed in a previous study of non-uniform growth lysozyme crystals by Dobrianov *et al.* (1998).

Acetylated lysozyme differs from its parent lysozyme mainly in terms of molecular charge, while both the modified and normal proteins are roughly the same in size and weight (Thomas & Chernov, 2001). Therefore, the incorporation of acetylated macromolecules into crystals may produce a type of substitutional disorder and results in microheterogeneity in the charge distribution. The combined X-ray topographic and high angular resolution diffraction results indicate that the incorporation of acetylated lysozyme molecules into lysozyme crystals facilitates formation of mosaic domains, although the crystal mosaicity may vary from one sample to another because of the varying amount of the impurities incorporated, the delicate nature of proteins and the complexity of crystallization. One can speculate that acetylation, which is meant to modify positively charged *R* groups such as lysine, might influence intermolecular binding at contact points in crystals which may result in the generation of mosaic blocks. No substantial difference in the FWHM of the radial-scan diffraction profiles along the reciprocal-lattice vectors has been observed between the nominally pure and impurity-incorporated crystals examined. Even for the highly mosaic and disordered crystal 3, the FWHM of the radial scan (Fig. 4*e*) is barely larger than that (Fig. 2*e*) from the lysozyme crystal 1, a high-quality crystal. In other words, the relative change in the lattice spacing of the reflection plane inside the impurity-doped crystals overall remains almost 'undetectable', although lattice orientation varies distinctly with different crystal parts as confirmed by X-ray topography. One probable explanation is that the overall impurity-induced lattice strain, which depends on how the impurities are distributed inside the crystals, is not sufficiently large to be strikingly observed with the low diffraction resolution reflections (the less strain-sensitive measurements) given that lysozyme and acetylated lysozyme molecules do not differ substantially in size and weight. Nevertheless, a lattice strain of, say, 3×10^{-4} would produce a peak broadening of ~3.5 arcsec (convoluted to a resulting diffraction profile) that is well within a resolving scale because of the high angular resolution used. A second likely reason for the above is that the stress or strain (Chernov, 1984, 1997, 1999) induced locally *via* the uptake of impurities is readily relieved by formation of dislocations and/or mosaic structures. This is presumably related to the intrinsically weak macromolecular bonding. A very recent study of space-grown

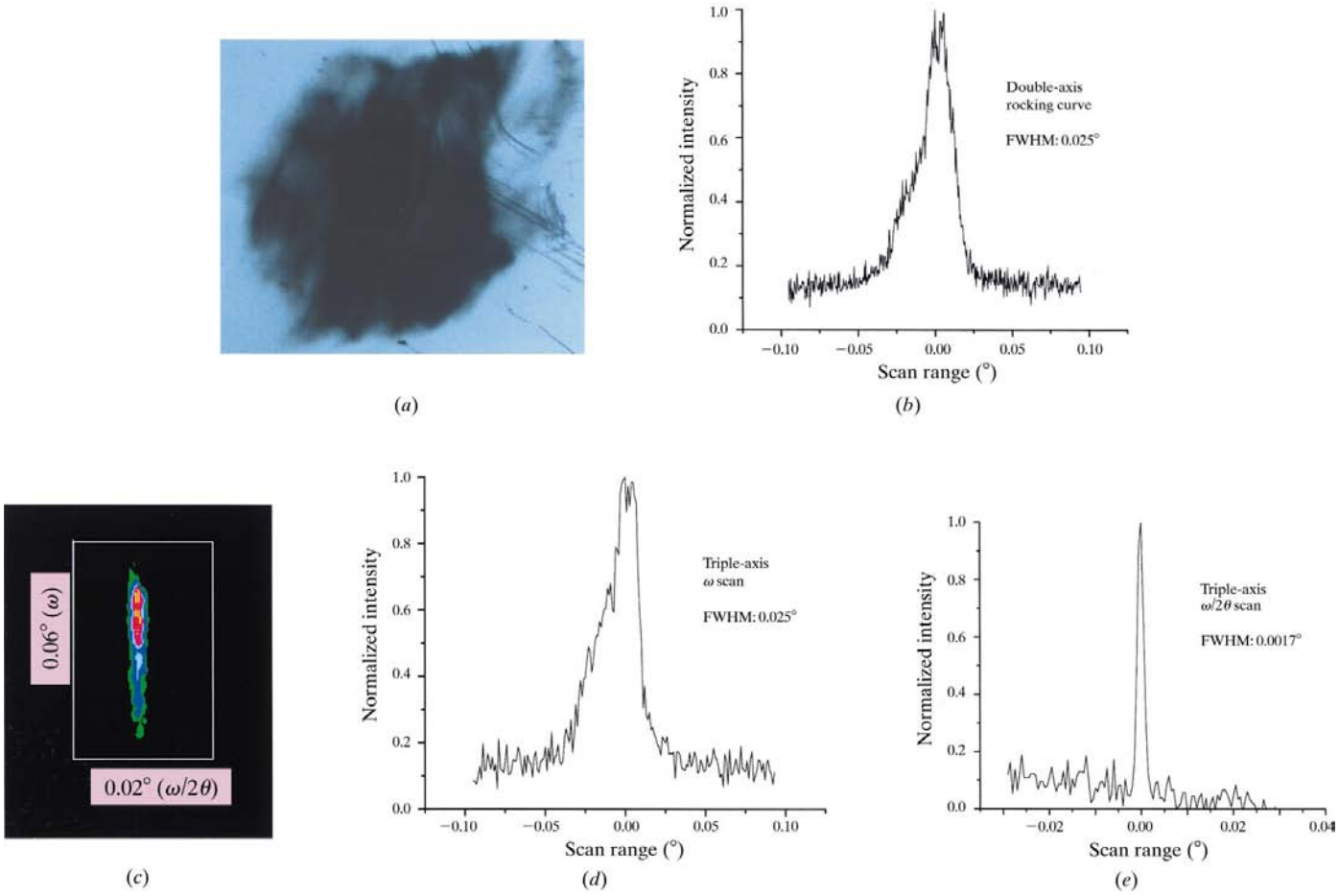

Figure 5
X-ray topographic and diffraction characterization of acetylated lysozyme doped lysozyme crystal 3. (*a*) X-ray topograph, (*b*) double-axis rocking curve, (*c*) triple-axis reciprocal-space map, (*d*) triple-axis ω scan, (*e*) triple-axis $\omega/2\theta$ scan. Curved streaks contaminate the upper-right corner of the diffraction image in (*a*).

and earth-grown lysozyme crystals (Boggon *et al.*, 2000) suggested that the weakness of macromolecular bonding should favor plastic flow in macromolecular crystals.

4. Concluding remarks

The present work has demonstrated that it is feasible and effective to undertake combined X-ray topography, double-axis rocking-curve and triple-axis high angular resolution diffraction-space mapping studies of structural imperfections in macromolecular crystals using laboratory X-ray sources. As pointed out by Helliwell (1992) and Bellamy *et al.* (2000), the rocking-curve width alone could be misleading in some cases because of the broadening effect of the instrumental function and possible experimental errors (Bowen & Tanner, 1998). However, although proper rocking-curve measurements and analyses may distinguish good crystals from bad crystals in terms of the values of FWHMs, they are unable to differentiate the mosaic spread from lattice strain and curvature because of the large angular acceptance used in 2θ (see, for example, Boggon *et al.*, 2000). With X-ray topography and triple-axis diffraction-space mapping, one can distinguish these effects. In the present case, the mutually misoriented mosaic domains rather than the lattice strain within the impurity-doped lysozyme crystals are primarily responsible for the broadening and splitting of the rocking curves of the reflections measured. The experimental results suggest that a change in the positively charged side chains on molecular surfaces affect intermolecular binding and ultimately the crystal quality, given that the modified and parent molecules do not differ significantly in size and weight, only in charge.

Laboratory X-ray characterization techniques can be explored further for the investigation of structural imperfections in macromolecular crystals. For example, with an optically well defined probe, diffuse scattering features from macromolecular crystals can be pinpointed in reciprocal space in the way that was used on inorganic crystals (Hu *et al.*, 1995) to investigate the origins of the diffuse scattering. By combining X-ray topography with diffraction-profile analysis, one can further distinguish the effect of lattice tilts from that of the dimensions of coherent domains and obtain more reliable information on the mosaic spread and the average size of domains (*e.g.* Hu *et al.*, 1999). This would in turn provide a better understanding of macromolecular crystal perfection and growth.

We would like to thank Drs E. H. Snell and M. L. Pusey for introducing and providing access to the X-ray diffraction system at Marshall Space Flight Center (MSFC), and Professor P. F. Fewster for fruitful discussions. ZWH is very grateful to Professor E. Meehan, Professor L. Q. Chen and Mrs A. Holmes *et al.* in the Laboratory for Structural Biology at University of Alabama in Huntsville, from whom he benefited considerably in the aspects of protein crystallography and crystallization. Mr D. Donovan and Mr D. Bennett are also thanked for their help and support. This work was supported by NASA under NAG 1454 and NASA/MSFC.

References

Bellamy, H. D., Snell, E. H., Lovelace, J., Pokross, M. & Borgstahl, G. E. O. (2000). *Acta Cryst.* D**56**, 986–995.
Boggon, T. J., Helliwell, J. R., Judge, R. A., Olczak, A., Siddons, D. P., Snell, E. H. & Stojanoff, V. (2000). *Acta Cryst.* D**56**, 868–880.
Bowen, D. K. & Tanner, B. K. (1998). *High-Resolution X-ray Diffractometry and Topography*. London: Taylor & Francis.
Carter, D. C., Lim, K., Ho, J. X., Wright, B. S., Twigg, P. D., Miller, T. Y., Chapman, J., Keeling, K., Ruble, J., Vekilov, P. G., Thomas, B. R., Rosenberger, F. & Chernov, A. A. (1999). *J. Cryst. Growth*, **196**, 623–637.
Caylor, C. L., Dobrianov, I., Lemay, S. G., Kimmer, C., Kriminski, S., Finkelstein, K. D., Zipfel, W., Webb, W. W., Thomas, B. R., Chernov, A. A. & Thorne, R. E. (1999). *Proteins Struct. Funct. Genet.* **36**, 270.
Chayen, N. E., Boggon, T. J., Cassetta, A., Deacon, A., Gleichmann, T., Habash, J., Harrop, S. J., Helliwell, J. R., Nieh, Y. P., Peterson, M. R., Raftery, J., Snell, E. H., Hadener, A., Niemann, A. C., Siddons, D. P., Stojanoff, V., Thompson, A. W., Ursby, T. & Wulff, N. (1996). *Quart. Rev. Biophys.* **29**, 227–278.
Chernov, A. A. (1984). *Modern Crystallography III: Crystal Growth. Springer Series of the Solid State*, Vol. 36. Berlin: Springer.
Chernov, A. A. (1997). *J. Cryst. Growth*, **174**, 354–361.
Chernov, A. A. (1999). *J. Cryst. Growth*, **196**, 524–534.
Dobrianov, I., Finkelstein, K. D., Lemay, S. G. & Thorne, R. E. (1998). *Acta Cryst.* D**54**, 922–937.
Durbin, S. D. & Feher, G. (1996). *Annu. Rev. Phys. Chem.* **47**, 171–204.
Fewster, P. F. (1996). *X-ray and Neutron Dynamical Diffraction: Theory and Applications*, edited by A. Authier, S. Lagomarsino & B. K. Tanner, pp. 269–287. New York: Plenum Press.
Fewster, P. F. (1997). *Crit. Rev. Solid State Mater. Sci.* **22**, 69–110.
Fourme, R., Ducruix, A., Ries-Kautt, M. & Capelle, B. (1995). *J. Synchrotron Rad.* **2**, 136.
Helliwell, J. R. (1988). *J. Cryst. Growth*, **90**, 259–272.
Helliwell, J. R. (1992). *Macromolecular Crystallography with Synchrotron Radiation*. Cambridge University Press.
Hu, Z. W., Thomas, P. A. & Risk, W. P. (1998). *Phys. Rev. B*, **58**, 6074–6080.
Hu, Z. W., Thomas, P. A. & Risk, W. P. (1999). *Phys Rev. B*, **59**, 14259–14264.
Hu, Z. W., Thomas, P. A. & Webjörn, J. (1995). *J. Phys. D*, **28**, A189–A194.
Hu, Z. W., Thomas, P. A. & Webjörn, J. (1996). *J. Appl. Cryst.* **29**, 279–284.
Judge, R. A., Snell, E. H., Pusey, M. L., Sportiello, M. G., Todd, P., Bellamy, H., Borgstahl, G. E. & Cassanto, J. M. (2000). Am. Crystallogr. Assoc. Meet. Abstr., p. 93.
Klapper, H. (1991). *Crystals: Growth, Properties and Applications*, Vol. 13, pp. 109–162. Berlin: Springer-Verlag.
Lang, A. R. (1976). *Modern Diffraction and Imaging Techniques in Materials Science*, Vol. II, edited by S. Amelincx, R. Gevers & J. van Landuyt, p. 623. Amsterdam: North Holland.
McPherson, A. (1998). *Crystallization of Biological Macromolecules.* Cold Spring Harbor, NY, USA: Cold Spring Harbor Laboratory Press.
McPherson, A., Malkin, A. J., Kuznetsov, Y. G., Koszelak, S., Wells, M., Jenkins G., Howard, J. & Lawson, G. (1999). *J. Cryst. Growth*, **196**, 572–586.
Ng, J. D., Lorber, B., Giegé, R., Koszelak, S., Day, J., Greenwood, A. & McPherson, A. (1997). *Acta Cryst.* D**53**, 724–733.
Otalora, F., Garcia-Ruiz, J. M., Gavira, J. A. & Capelle, B. (1999). *J. Cryst. Growth*, **196**, 546–558.

Rosenberger, F., Vekilov, P. G., Muschol, M. & Thomas, B. R. (1996). *J. Cryst. Growth*, **168**, 1–27.
Shaikevitch, A. & Kam, Z. (1981). *Acta Cryst.* A**37**, 871–875.
Snell, E. H., Fewster, P. F., Norman, A., Boggon, T. J., Judge, R. A. & Pusey, M. L. (1999). XVIII IUCr Congr. Assembly Abstr., p. 546.
Snell, E. H., Weisgerber, S., Helliwell, J. R., Weckert, E., Holzer, K. & Schroer, K. (1995). *Acta Cryst.* D**51**, 1099–1102.
Stojanoff, V. & Siddons, D. P. (1996). *Acta Cryst.* A**52**, 498–499.
Stojanoff, V., Siddons, D. P., Monaco, L. A., Vekilov, P. & Rosenberger, F. (1997). *Acta Cryst.* D**53**, 588–595.
Tanner, B. K. (1976). *X-ray Diffraction Topography*. Oxford: Pergamon.
Thomas, B. R. & Chernov, A. A. (2001). In the press.
Thomas, B. R., Vekilov, P. G. & Rosenberger, F. (1996). *Acta Cryst.* D**52**, 776–784.
Thomas, B. R., Vekilov, P. G. & Rosenberger, F. (1998). *Acta Cryst.* D**54**, 226–236.
Volz, H. M. & Matyi, R. J. (1999). *Philos. Trans. R. Soc. London Ser. A*, **357**, 2789–2799.
Volz, H. M. & Matyi, R. J. (2000). *Acta Cryst.* D**56**, 881–888.